Electronic Supplementary Information

Experimental section

Materials: Sodium Tungstate Dihydrate ($Na_2WO_4 \cdot 2H_2O$), Nickel foam (NF), Ammonium sulfate ($(NH_4)_2SO_4$), Nickel sulfate ($NiSO_4$), Sodium sulfate (Na_2SO_4), anhydrous ethanol (C_2H_6O), ammonium chloride (NH_4Cl), sodium hydroxide (NaOH), salicylic acid ($C_7H_6O_3$), sodium citrate dihydrate ($C_6H_5Na_3O_7 \cdot 2H_2O$), p–dimethylamino benzaldehyde ($C_9H_{11}NO$), and sodium nitroferricyanide dihydrate ($C_5FeN_6Na_2O \cdot 2H_2O$) were purchased from Chengdu Kelong Ltd.

Preparation of WO_3/NF: Typically, 0.184 g of $Na_2WO_4 \cdot 2H_2O$ and 0.3 g of $(NH_4)_2SO_4$ were dissolved in 15 mL of deionized water, respectively, and then mixed with slow stirring for one hour. Finally, the product was transferred to a 50 ml sealed Teflon-lined stainless steel autoclave. Subsequently, The Nickel foam (NF) was ultrasonically cleaned with acetone, ethanol, and deionized water for 10 min and dried in air. And, the cleaned NF was placed in the solution in the autoclave. Then the autoclave was kept at 160 °C for 16 h. After the autoclave cooled down at room temperature, the NF was taken out and washed with water and ethanol several times and subsequently dried at 60 ºC overnight.

Preparation of WO_2/NF: The precursor WO_3/NF was put into a tubular furnace, and argon hydrogen atmosphere was injected into the furnace for 30 minutes, the heating rate was 5 ℃/min, and the heat preservation was held at 650 ℃ for 0.5 h.

Preparation of Ni@WO_2/NF: WO_2/NF electrodes were electroplated with 0.13 M $NiSO_4$, 0.13 M Na_2SO_4, and 0.1 M $C_6H_5Na_3O_7 \cdot 2H_2O$ at a current density of 10 mA cm^{-2} and plating time of 180 s.

Characterizations: The crystal structure of the prepared material was determined

using an X-ray diffractometer with Cu Kα radiation (DX-2700B). microstructural observations were performed on a field−emission scanning electron microscopy (FEI Insect F50) and an atomic resolution scanning transmission electron microscopy (FEI Talos F200S Super). XPS measurements were carried out with Thermo Fischer ESCALAB Xi^+. The absorbance data were measured via an Ultraviolet-visible (UV–Vis) spectrophotometer (Shimazu UV–2600). EPR spectrum was recorded on a Brüker EMX spectrometer at room temperature.

Electrochemical measurements: All electrochemical measurements were carried out in an H−shaped cell separated by a Nafion 117 membrane using a CHI 760E electrochemical workstation (Chenhua, Shanghai). The area of the working electrode immersed in the electrolyte is 0.25 cm^2. LSV was performed in Ar−saturated 0.1 M NaOH with 0.1 M $NaNO_2$ at a scan rate of 5 mV s^{-1}. All potentials reported in this work were converted to a reversible hydrogen electrode (RHE) scale, and current densities were normalized to the geometric surface area. All experiments were carried out at room temperature (25 °C).

Determination of NH_3: The NH_3 concentration in the electrolyte was determined (the obtained electrolyte was diluted 50 times) by the indophenol blue method. Specifically, 2 mL of electrolyte collected after electrolysis was mixed with 2 mL of coloring solution (1 M NaOH containing 5% salicylic acid and 5% sodium citrate), and 1 mL of oxidizing solution (0.05 M NaClO). Then 0.2 mL oxidation solution (0.05 M NaClO) mL catalyst solution (1 wt% $C_5FeN_6Na_2O$ $2H_2O$) was dropped into the collected solution. After standing in the dark for 2 h, the concentration of NH_3 was determined by UV-Vis at a specific wavelength of 655 nm. The concentration−absorbance curve was calibrated using the standard NH_4Cl solution

with known concentrations of 0.0, 0.25, 0.5, 1.0, 1.5, 2.0, and 2.5 μg mL^{-1} in 0.1 M NaOH. The fitting curve ($y = 0.41927x + 0.02789$, $R^2 = 0.9998$) shows a good linear relation of absorbance value with NH_3 concentration.

Determination of NH_3 yield and FE:

The NH_3 FE is estimated from the charge consumed for NO_2^- reduction and the total charge passed through the electrode:

$$FE = 6 \times F \times V \times [NH_3] / (Q \times 17) \times 100\%$$

The yield rate of NH_3 (aq) is calculated:

$$NH_3 \text{ yield} = V \times [NH_3] / (A \times t \times 17)$$

Where $[NH_3]$ is the concentration of NH_3 (aq), F is the Faradaic constant (96485 C mol^{-1}), V is the volume of electrolyte in the anode compartment (45 mL), Q is the total charge passing the electrode, t is the electrolysis time, and A is the geometric surface area.

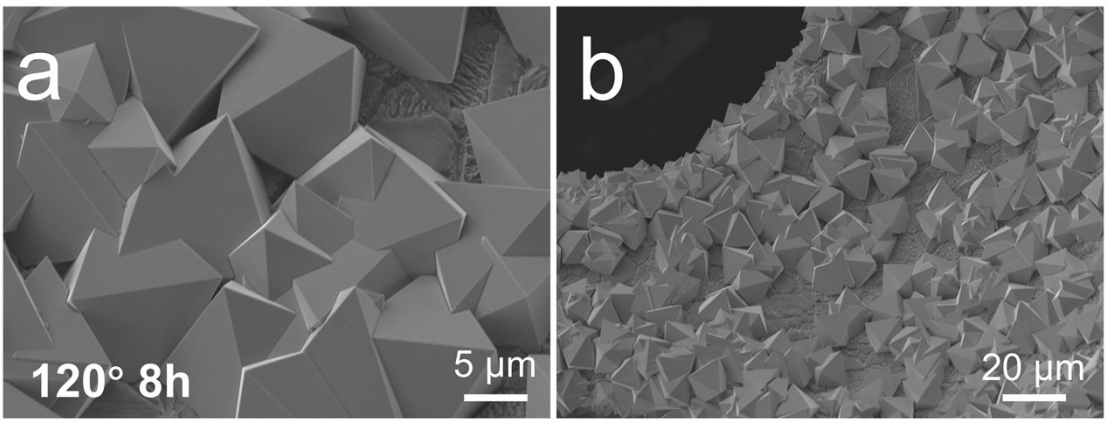

Fig. S1. 120 ℃ for 8 h SEM images of WO_3/NF.

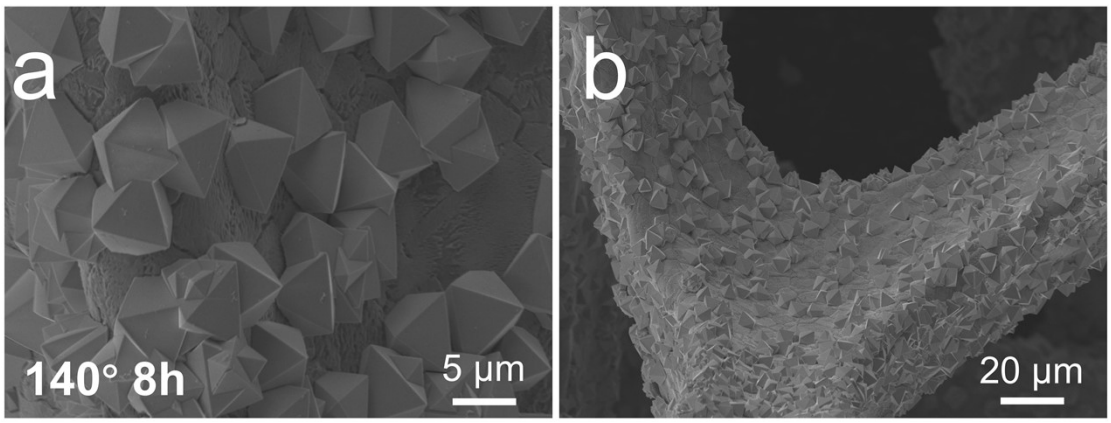

Fig. S2. 140 ℃ for 8 h SEM images of WO_3/NF.

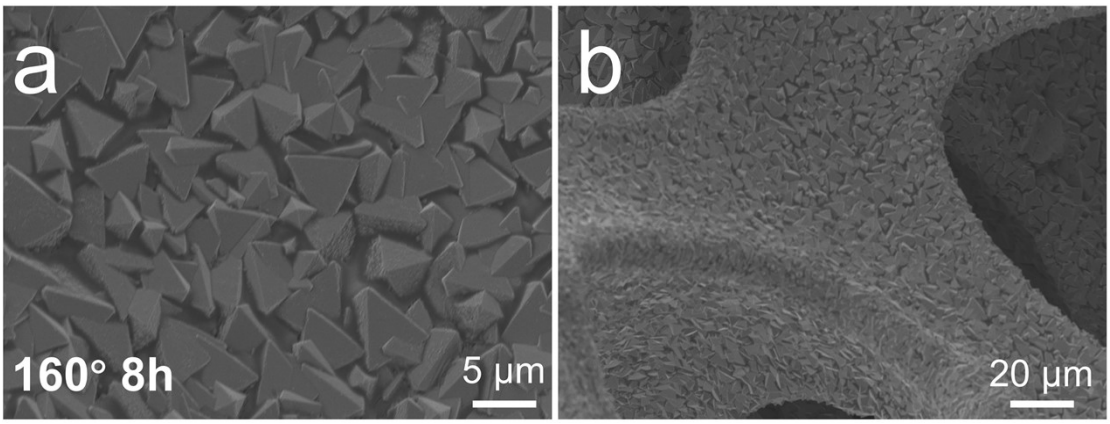

Fig. S3. 160 ℃ for 8 h SEM images of WO_3/NF.

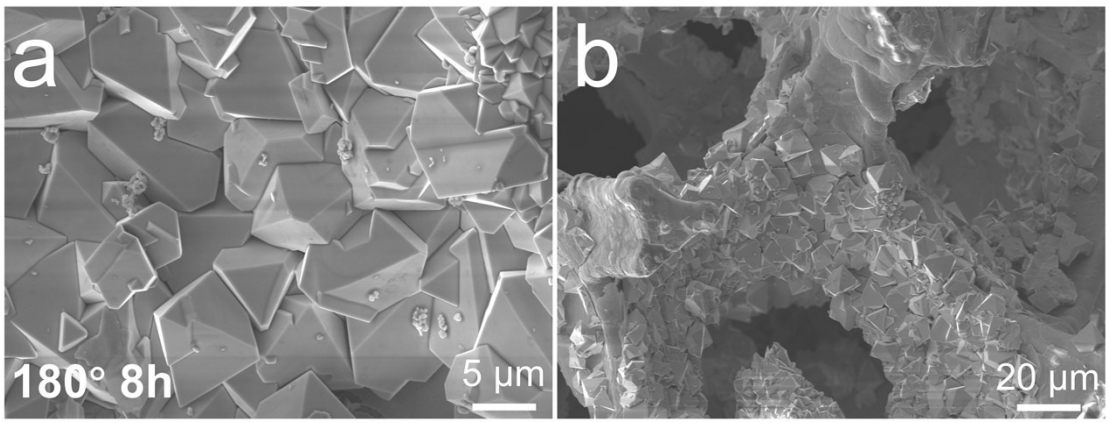

Fig. S4. 180 ℃ for 8 h SEM images of WO_3/NF.

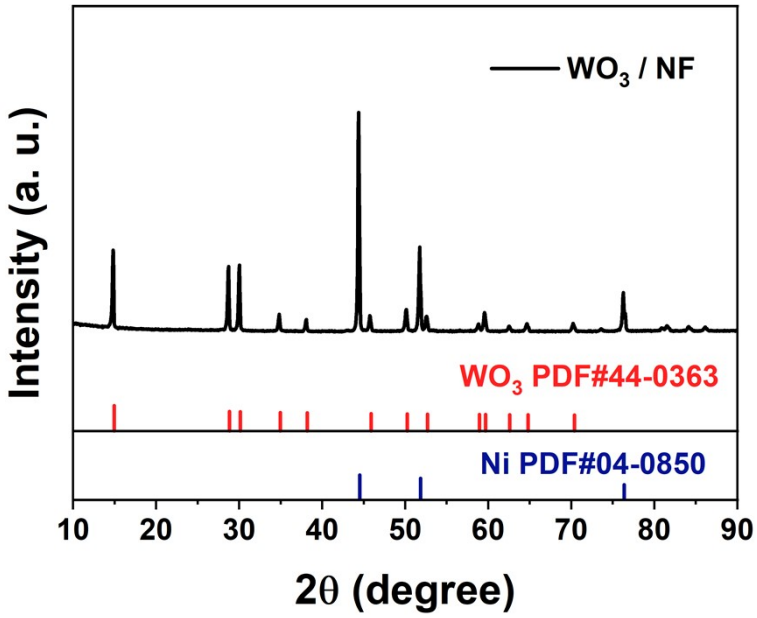

Fig. S5. 160 ℃ for 16 h XRD pattern of WO_3/NF.

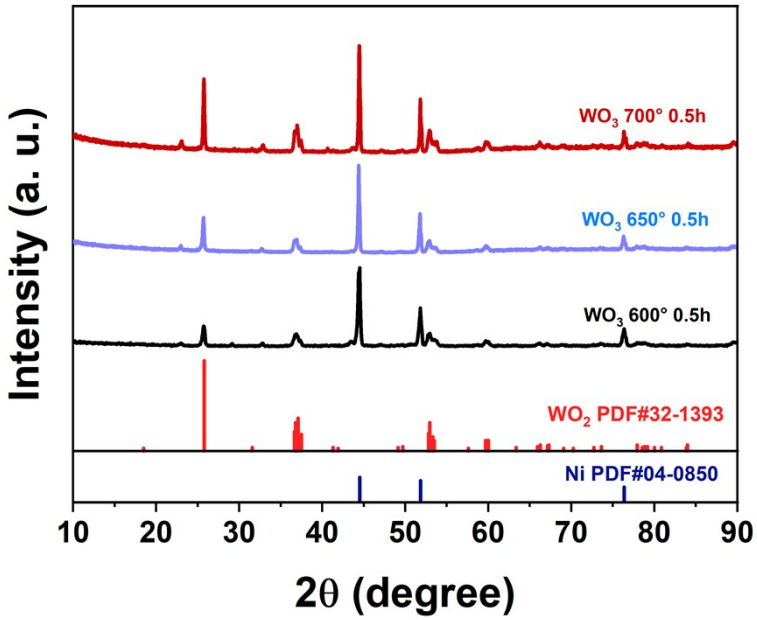

Fig. S6. XRD pattern of WO_2/NF at different calcination temperatures.

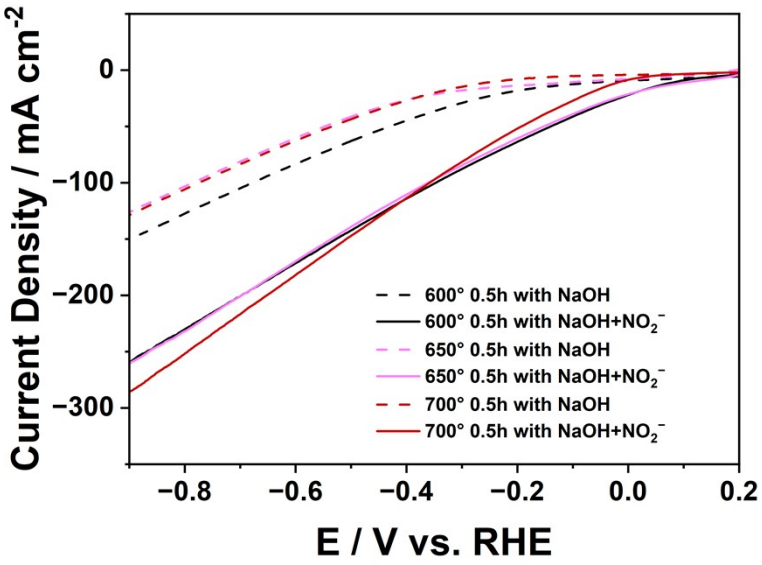

Fig. S7. LSV curves of WO_2/NF at different temperatures.

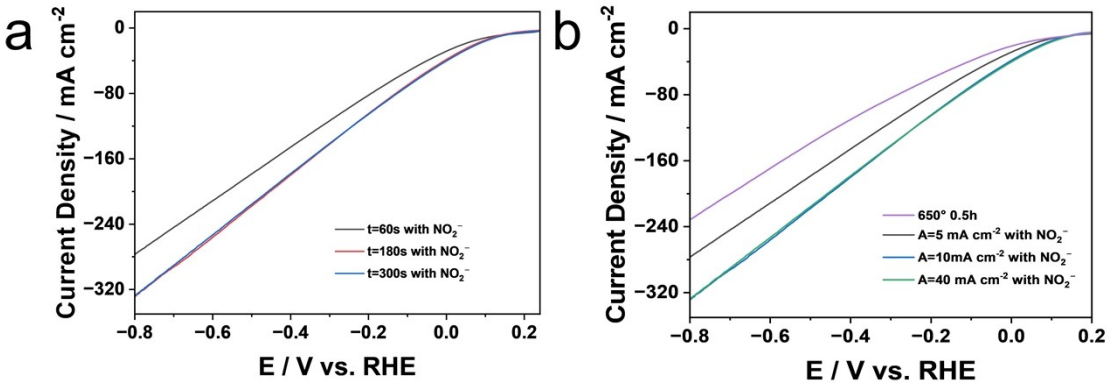

Fig. S8. (a) LSV curves of Ni@WO_2/NF at different electrodeposition current densities. (b) Press the LSV curve of Ni@WO_2/NF for different electrodeposition times.

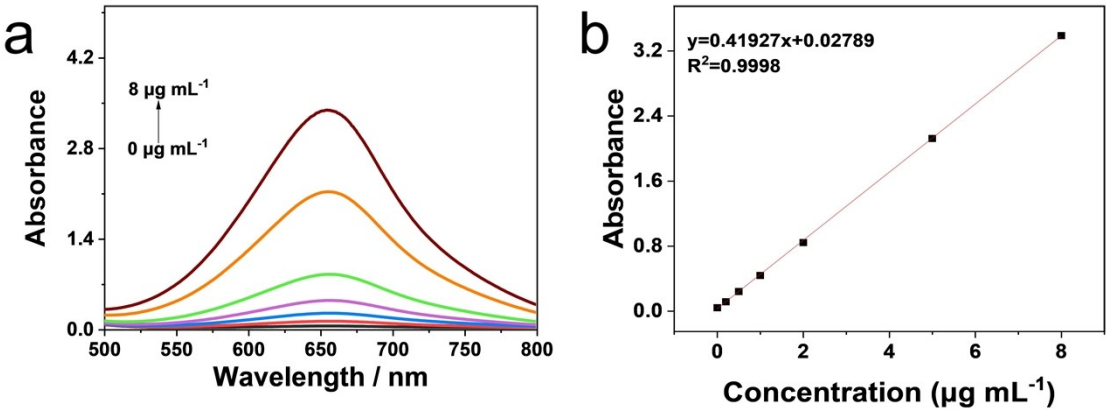

Fig. S9. (a) UV−Vis spectra and (b) corresponding calibration curves were used to calculate NH_4^+.

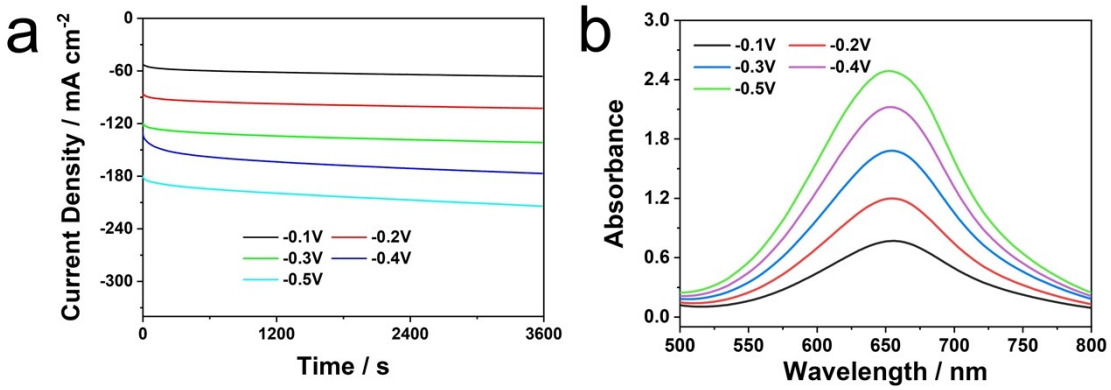

Fig. S10. (a) Chronoamperometry curves and (b) corresponding UV-Vis spectra of Ni@WO_2/NF from −0.1 V to −0.5 V.

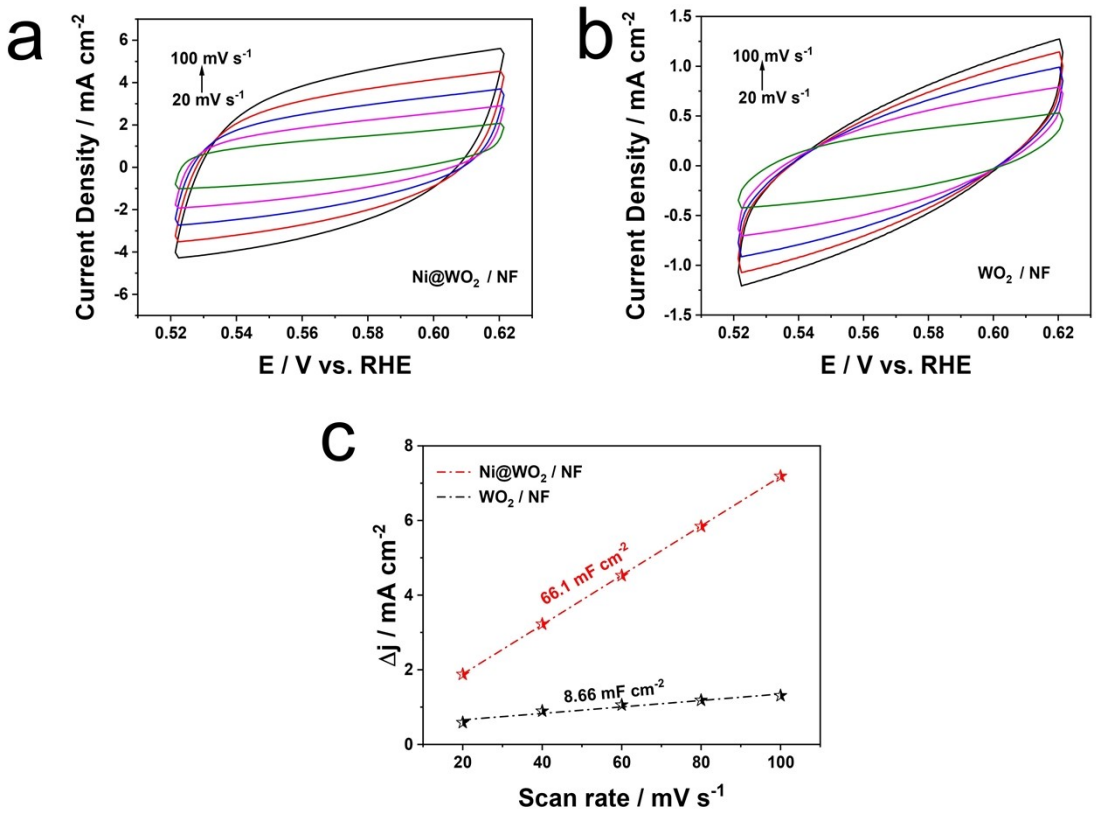

Fig. S11. CV curves of WO_2/NF (a), Ni@WO_2/NF (b) at different scan rates (20−100 mV s^{-1}). (c)The double−layer capacitance (Cdl) for Ni@WO_2/NF, and WO_2/NF, respectively. Cdl is proportional to the electrochemical surface area (ECSA).

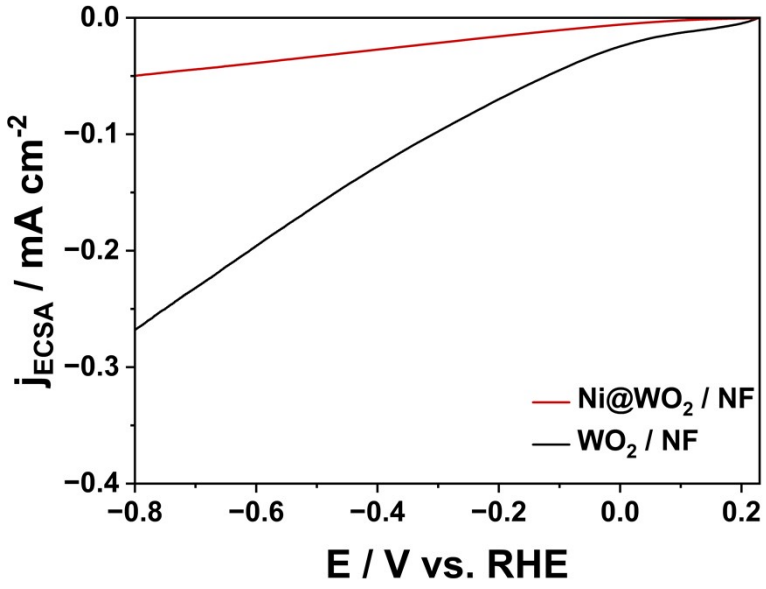

Fig. S12. ECSA−normalized current densities of Ni@WO_2/NF and WO_2/NF.

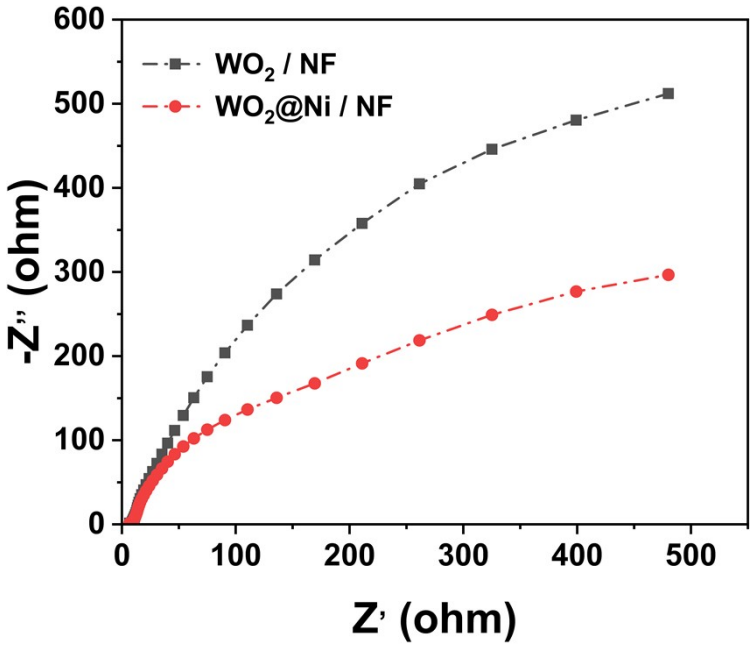

Fig. S13. Electrochemical impedance spectroscopy (EIS) for Ni@WO_2/NF, and WO_2/NF, respectively.

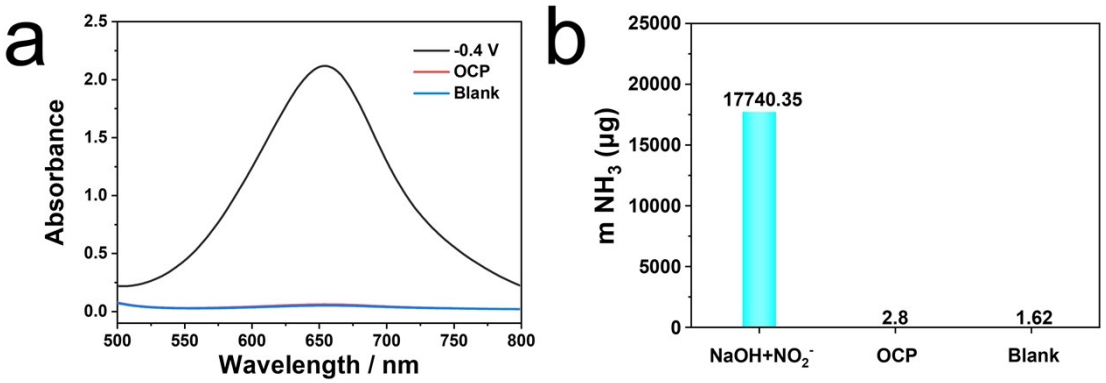

Fig. S14. (a) UV−Vis spectra and (b) amounts of electrogenerated NH_3 under different operating conditions.

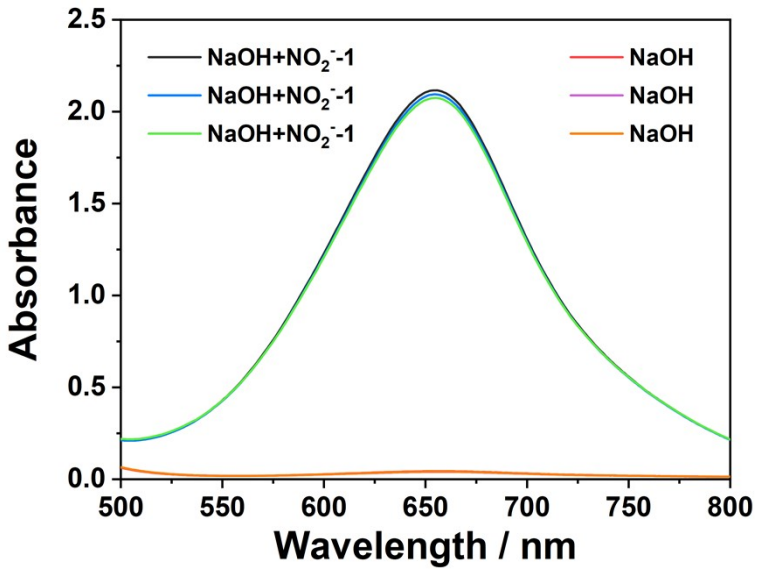

Fig. S15. UV-absorbable spectra of Ni@WO_2/NF are tested alternately in a 0.1 M NaOH electrolyte with and without $NaNO_2$ and without $NaNO_2$.

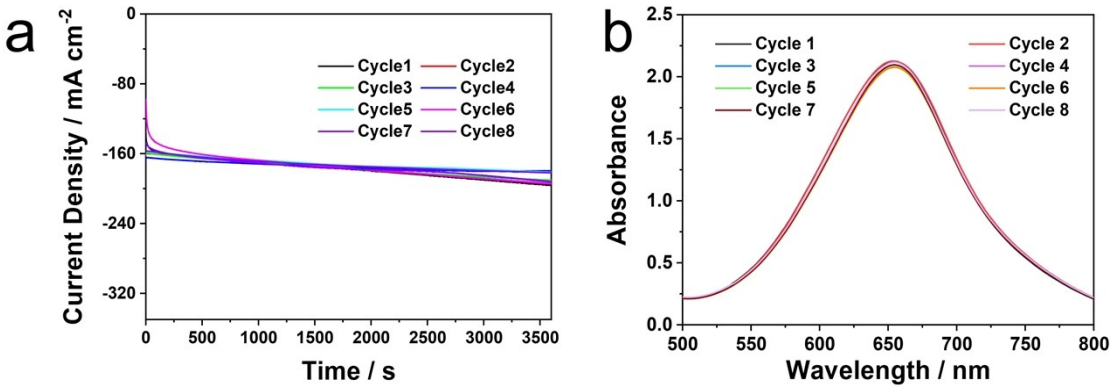

Fig. S16. (a) Chronoamperometry curves and (b) corresponding UV−Vis absorption spectra of Ni@WO_2/NF for electrochemical catalytic production of NH_3 during cycling tests in 0.1 M NaOH with 0.1 M NO_2^- at −0.4V.

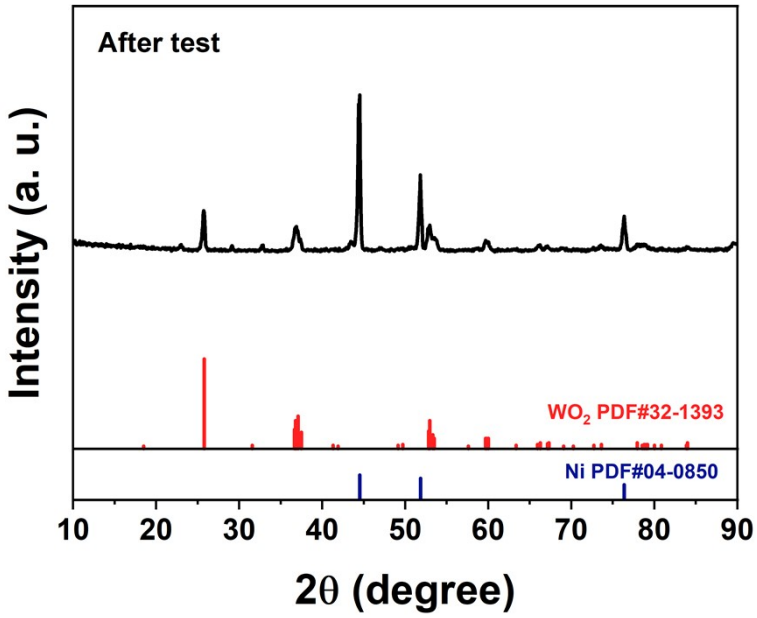

Fig. S17. XRD of Ni@WO_2/NF after long electrolysis.

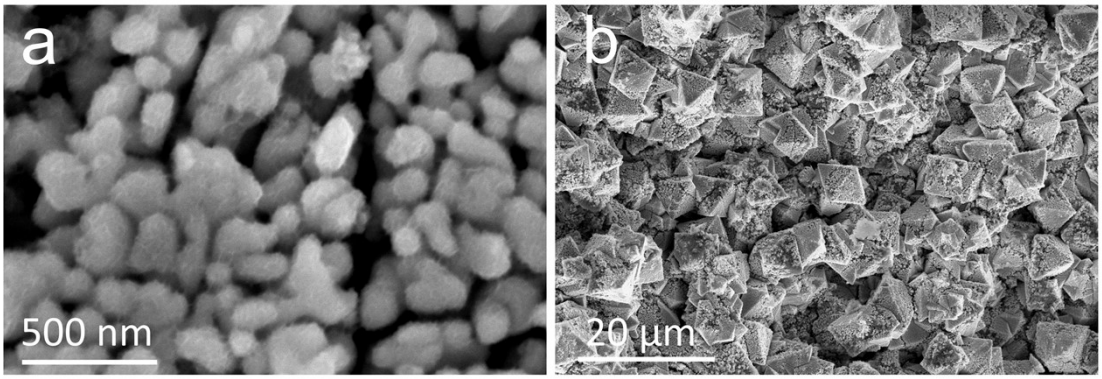

Fig. S18. SEM images of Ni@WO_2/NF after long-term electrolysis.

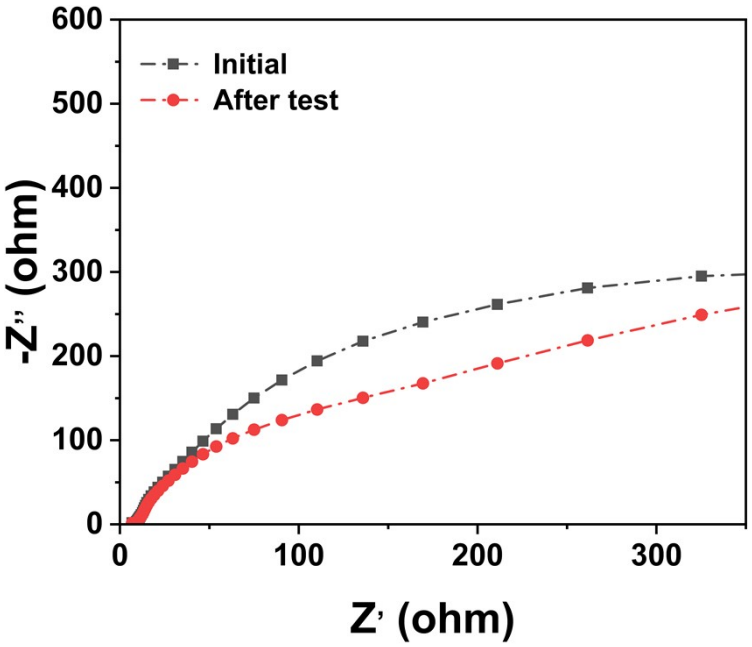

Fig. S19. EIS before and after stability test.

Table S1. Comparison of catalytic performance of Ni@WO_2/NF with other reported NO_2^-RR electrocatalysts.

Catalyst	Electrolyte	FE (%)	NH_3 yield rate	Refs.
Ni@WO_2/NF	**0.1 M NaOH (0.1 M $NaNO_2$)**	**94.6**	**17959.3 μg h^{-1} cm^{-2} (1056.43 μmol cm^{-2})**	**This work**
Ag@NiO	0.1 M NaOH (0.1 M $NaNO_2$)	97.7	5751 μg h^{-1} cm^{-2}	1
C-$NiWO_4$	0.1 M NaOH (0.1 M $NaNO_2$)	97.6	10974.36 μg h^{-1} cm^{-2}	2
Ag@TiO_2	0.1 M NaOH (0.1 M $NaNO_2$)	96.4	8743.1 μg h^{-1} cm^{-2}	3
Ni@TiO_2	0.1 M NaOH (0.1 M $NaNO_2$)	98.5	9667.9 μg h^{-1} cm^{-2}	4
NiS_2@TiO_2	0.1 M NaOH (0.1 M $NaNO_2$)	92.1	10062.3 μg h^{-1} cm^{-2}	5
Ni-TiO_2	0.1 M NaOH (0.1 M $NaNO_2$)	94.9	6464.6 μg h^{-1} cm^{-2}	6
Cu/JDC	0.1 M NaOH (0.1 M $NaNO_2$)	93.2	8899.5 μg h^{-1} cm^{-2}	7
V-TiO_2	0.1 M NaOH (0.1 M $NaNO_2$)	93.2	7083.9 μg h^{-1} cm^{-2}	8
A-TiO_{2x}	0.1 M NaOH (0.1 M $NaNO_2$)	91.1	12230.1 μg h^{-1} cm^{-2}	9
WO_2	0.1 M NaOH (0.1 M $NaNO_2$)	94.3	14964.25 μg h^{-1} cm^{-2}	10
FEOOH NTA	0.1 M NaOH (0.1 M $NaNO_2$)	94.7	11937 μg h^{-1} cm^{-2}	11
Ni−NSA−V_{Ni}	0.2 M Na_2SO_4 (200 ppm NO_2^-)	88.9	235.98 μmol h^{-1} cm^{-2}	12
Cobalt-tripeptide complex	1.0 M MOPS buffer (1.0 M $NaNO_2$)	90±3	3.01 × 10^{-10} mol s^{-1} cm^{-2}	13
Poly-NiTRP complex	$NaNO_2$ (0.1 M $NaClO_4$)	—	1.1 mM	14
FeN_5H_2	1.0 M MOPS (1.0 M $NaNO_2$)	> 90	—	15
Cu_3P NA/CF	0.1 M PBS (0.1 M $NaNO_2$)	91.2 ± 2.5	1626.6 μg h^{-1} cm^{-2}	16

Table S2. Comparison of NH_3 yield and power density of our battery with recent Zn-N_2, Zn-NO, Zn-NO_2^-, or Zn-NO_3^- battery systems.

Catalyst	Battery Type	Power density (mW cm^{-2})	Refs.
Ni@WO_2/NF	**Zn-NO_2^-**	**9.05**	**This work**
Cu NDs	Zn-N_2	0.0101	17
FeHTNs	Zn-N_2	0.01642	18
VN@NSC	Zn-N_2	0.01642	19
CoPi/HSNPC	Zn-N_2	0.31	20
NbS_2	Zn-N_2	0.31	21
CoPi/NPCS	Zn-N_2	0.49	22
Ti_2O_3	Zn-N_2	1.02	23
$FePS_3$	Zn-N_2	2.6	24
CoP	Zn-NO	0.496	25
NiO	Zn-NO	0.88	26
MoS_2	Zn-NO	1.04	27
Fe_2O_3	Zn-NO	1.18	28
Ni_2P	Zn-NO	1.53	29
TiO_2@Ti	Zn-NO	1.7	30
MoC	Zn-NO	1.8	31
VN	Zn-NO	2.0	32
CoS	Zn-NO	2.06	33
BiNDs	Zn-NO	2.33	34
Bi@C	Zn-NO	2.35	35
ITO@TiO_2TP	Zn-NO_2^-	1.22	36
A-TiO_{2-x}	Zn-NO_2^-	2.38	37
TiO_2	Zn-NO_3^-	0.87	38
Fe/Ni_2P	Zn-NO_3^-	3.25	39
Co_2AlO_4	Zn-NO_3^-	3.43	40
CeO_2	Zn-NO_3^-	3.44	41
$NiCo_2O_4$	Zn-NO_3^-	3.94	42

References

1 Q. Liu, G. Wen, D. Zhao, L. Xie, S. Sun, L. Zhang, Y. Luo, A. Ali Alshehri, M.S. Hamdy, Q. Kong, X. Sun, Nitrite reduction over Ag nanoarray electrocatalyst for ammonia synthesis, *Journal of Colloid and Interface Science* **623** (2022) 513-519.

2 H. Qiu, Q. Chen, J. Zhang, X. An, Q. Liu, L. Xie, W. Yao, X. Sun, Q. Kong, $NiWO_4$ nanoparticles with oxygen vacancies: high-efficiency electrosynthesis of ammonia with selective reduction of nitrite, *Inorganic Chemistry Frontiers* **10** (2023) 3909-3915.

3 X. Fan, X. He, X. Ji, L. Zhang, J. Li, L. Hu, X. Li, S. Sun, D. Zheng, Y. Luo, Y. Wang, L. Xie, Q. Liu, B. Ying, X. Sun, High-efficiency electrosynthesis of ammonia with selective reduction of nitrite over an Ag nanoparticle-decorated TiO_2 nanoribbon array, *Inorganic Chemistry Frontiers* **10** (2023) 1431-1435.

4 X. Ji, C. Ma, F. Zhang, X. He, X. Fan, J. Li, Z. Li, L. Ouyang, L. Zhang, T. Li, D. Zhao, Y. Wang, J. Zhang, Z. Cai, S. Sun, A.A. Alshehri, Q. Lu, X. Sun, Ni@TiO2 Nanoarray with the Schottky Junction for the Highly Selective Electrochemical Reduction of Nitrite to Ammonia, *ACS Sustainable Chemistry & Engineering* **11** (2023) 2686-2691.

5 X. He, L. Hu, L. Xie, Z. Li, J. Chen, X. Li, J. Li, L. Zhang, X. Fang, D. Zheng, S. Sun, J. Zhang, A. Ali Alshehri, Y. Luo, Q. Liu, Y. Wang, X. Sun, Ambient ammonia synthesis via nitrite electro reduction over NiS_2 nanoparticles-

decorated TiO_2 nanoribbon array, *Journal of Colloid and Interface Science* **634** (2023) 86-92.

6 Z. Cai, C. Ma, D. Zhao, X. Fan, R. Li, L. Zhang, J. Li, X. He, Y. Luo, D. Zheng, Y. Wang, B. Ying, S. Sun, J. Xu, Q. Lu, X. Sun, Ni doping enabled improvement in electrocatalytic nitrite-to-ammonia conversion over TiO_2 nanoribbon, *Materials Today Energy* **31** (2023).

7 L. Ouyang, L. Yue, Q. Liu, Q. Liu, Z. Li, S. Sun, Y. Luo, A. Ali Alshehri, M.S. Hamdy, Q. Kong, X. Sun, Cu nanoparticles decorated juncus-derived carbon for efficient electrocatalytic nitrite-to-ammonia conversion, *Journal of Colloid and Interface Science* **624** (2022) 394-399.

8 H. Wang, F. Zhang, M. Jin, D. Zhao, X. Fan, Z. Li, Y. Luo, D. Zheng, T. Li, Y. Wang, B. Ying, S. Sun, Q. Liu, X. Liu, X. Sun, V-doped TiO_2 nanobelt array for high-efficiency electrocatalytic nitrite reduction to ammonia, *Materials Today Physics* **30** (2023).

9 Z. Ren, Q. Chen, X. An, Q. Liu, L. Xie, J. Zhang, W. Yao, M.S. Hamdy, Q. Kong, X. Sun, High-Efficiency Ammonia Electrosynthesis on Anatase TiO_{2-x} Nanobelt Arrays with Oxygen Vacancies by Selective Reduction of Nitrite, *Inorganic Chemistry* **61** (2022) 12895-12902.

10 H. Qiu, Q. Chen, X. An, Q. Liu, L. Xie, J. Zhang, W. Yao, Y. Luo, S. Sun, Q. Kong, J. Chen, X. Sun, WO_2 nanoparticles with oxygen vacancies: a high-efficiency electrocatalyst for the conversion of nitrite to ammonia, *Journal of Materials Chemistry A* **10** (2022) 24969-24974.

11 Q. Liu, Q. Liu, L. Xie, L. Yue, T. Li, Y. Luo, N. Li, B. Tang, L. Yu, X. Sun, A 3D FeOOH nanotube array: an efficient catalyst for ammonia electrosynthesis by nitrite reduction, *Chemical Communications* **58** (2022) 5160-5163.

12 C. Wang, W. Zhou, Z. Sun, Y. Wang, B. Zhang and Y. Yu, *J. Mater. Chem. A*, 2021, **9**, 239-243.

13 Y. Guo, J. R. Stroka, B. Kandemir, C. E. Dickerson and K. L. Bren, *J. Am. Chem. Soc.*, 2018, **140**, 16888-16892.

14 P. Dreyse, M. Isaacs, K. Calfumán, C. Cáceres, A. Aliaga, M. J. Aguirre and D. Villagra, *Electrochim. Acta*, 2011, **56**, 5230-5237.

15 J. R. Stroka, B. Kandemir, E. M. Matson and K. L. Bren, *ACS Catal.*, 2020, **10**, 13968-13972.

16 J. Liang, B. Deng, Q. Liu, G. Wen, Q. Liu, T. Li, Y. Luo, A. A. Alshehri, K. A. Alzahrani and D. Ma, *Green Chem.*, 2021, **23**, 5487-5493.

17 C. Du, Y. Gao, J. Wang and W. *Chem. Commun.*, 2019, **55**, 12801-12804.

18 X.-W. Lv, X.-L. Liu, L.-J. Gao, Y.-P. Liu and Z.-Y. Yuan, *J. Mater. Chem. A*, 2021, **9**, 4026-4035.

19 X.-W. Lv, Y. Liu, Y.-S. Wang, X.-L. Liu and Z.-Y. Yuan, *Appl. Catal. B*, 2021, **280**, 119434.

20 J.-T. Ren, L. Chen, Y. Liu and Z.-Y. Yuan, *J. Mater. Chem. A*, 2021, **9**, 11370-11380.

21 H. Wang, J. Si, T. Zhang, Y. Li, B. Yang, Z. Li, J. Chen, Z. Wen, C. Yuan, L. Lei and Y. Hou, *Appl. Catal. B*, 2020, **270**, 118892.

22 J. T. Ren, L. Chen, H. Y. Wang and Z. Y. Yuan, *ACS Appl. Mater. Interfaces*, 2021, **13**, 12106-12117.

23 H.-j. Chen, Z.-q. Xu, S. Sun, Y. Luo, Q. Liu, M. S. Hamdy, Z.-s. Feng, X. Sun and Y. Wang, *Inorg. Chem. Front.*, 2022, **9**, 4608-4613.

24 H. Wang, Z. Li, Y. Li, B. Yang, J. Chen, L. Lei, S. Wang and Y. Hou, *Nano Energy*, 2021, **81**.

25 J. Liang, W.-F. Hu, B. Song, T. Mou, L. Zhang, Y. Luo, Q. Liu, A. A. Alshehri, M. S. Hamdy, L.-M. Yang and X. Sun, *Inorg. Chem. Front.*, 2022, **9**, 1366-1372.

26 P. Liu, J. Liang, J. Wang, L. Zhang, J. Li, L. Yue, Y. Ren, T. Li, Y. Luo, N. Li, B. Tang, Q. Liu, A. M. Asiri, Q. Kong and X. Sun, *Chem. Commun.*, 2021, **57**, 13562-13565.

27 L. Zhang, J. Liang, Y. Wang, T. Mou, Y. Lin, L. Yue, T. Li, Q. Liu, Y. Luo, N. Li, B. Tang, Y. Liu, S. Gao, A. A. Alshehri, X. Guo, D. Ma and X. Sun, *Angew. Chem. Int. Ed*, 2021, **60**, 25263-25268.

28 J. Liang, H. Chen, T. Mou, L. Zhang, Y. Lin, L. Yue, Y. Luo, Q. Liu, N. Li, A. A. Alshehri, I. Shakir, P. O. Agboola, Y. Wang, B. Tang, D. Ma and X. Sun, *J. Mater. Chem. A*, 2022, **10**, 6454-6462.

29 T. Mou, J. Liang, Z. Ma, L. Zhang, Y. Lin, T. Li, Q. Liu, Y. Luo, Y. Liu, S. Gao, H. Zhao, A. M. Asiri, D. Ma and X. Sun, *J. Mater. Chem. A*, 2021, **9**, 24268-24275.

30 J. Liang, P. Liu, Q. Li, T. Li, L. Yue, Y. Luo, Q. Liu, N. Li, B. Tang, A. A.

Alshehri, I. Shakir, P. O. Agboola, C. Sun and X. Sun, *Angew. Chem. Int. Ed*, 2022, **61**, e202202087.

31 G. Meng, M. Jin, T. Wei, Q. Liu, S. Zhang, X. Peng, J. Luo and X. Liu, *Nano Res.*, 2022, DOI: 10.1007/s12274-022-4747-y.

32 D. Qi, F. Lv, T. Wei, M. Jin, G. Meng, S. Zhang, Q. Liu, W. Liu, D. Ma, M. S. Hamdy, J. Luo and X. Liu, *Nano Res. Energy*, 2022, **1,** e9120022.

33 L. Zhang, Q. Zhou, J. Liang, L. Yue, T. Li, Y. Luo, Q. Liu, N. Li, B. Tang, F. Gong, X. Guo and X. Sun, *Inorg. Chem.*, 2022, **61**, 8096-8102.

34 Y. Lin, J. Liang, H. Li, L. Zhang, T. Mou, T. Li, L. Yue, Y. Ji, Q. Liu, Y. Luo, N. Li, B. Tang, Q. Wu, M. S. Hamdy, D. Ma and X. Sun, *Mater. Today Phys.*, 2022, **22**.

35 Q. Liu, Y. Lin, L. Yue, J. Liang, L. Zhang, T. Li, Y. Luo, M. Liu, J. You, A. A. Alshehri, Q. Kong and X. Sun, *Nano Res.*, 2022, **15**, 5032-5037.

36 S. Li, J. Liang, P. Wei, Q. Liu, L. Xie, Y. Luo and X. Sun, *eScience*, 2022, **2**, 382-388.

37 Z. Ren, Q. Chen, X. An, Q. Liu, L. Xie, J. Zhang, W. Yao, M. S. Hamdy, Q. Kong and X. Sun, *Inorg. Chem.*, 2022, **61**, 12895-12902.

38 Y. Guo, R. Zhang, S. Zhang, Y. Zhao, Q. Yang, Z. Huang, B. Dong and C. Zhi, *Energy Environ. Sci.*, 2021, **14**, 3938-3944.

39 R. Zhang, Y. Guo, S. Zhang, D. Chen, Y. Zhao, Z. Huang, L. Ma, P. Li, Q. Yang, G. Liang and C. Zhi, *Adv. Energy Mater.*, 2022, **12**.

40 Z. Deng, J. Liang, Q. Liu, C. Ma, L. Xie, L. Yue, Y. Ren, T. Li, Y. Luo, N. Li,

B. Tang, A. Ali Alshehri, I. Shakir, P. O. Agboola, S. Yan, B. Zheng, J. Du, Q. Kong and X. Sun, *Chem. Eng. J.*, 2022, **435**.

41 Z. Li, Z. Deng, L. Ouyang, X. Fan, L. Zhang, S. Sun, Q. Liu, A. A. Alshehri, Y. Luo, Q. Kong and X. Sun, *Nano Res.*, 2022, DOI: 10.1007/s12274-022-4863-8.

42 Q. Liu, L. Xie, J. Liang, Y. Ren, Y. Wang, L. Zhang, L. Yue, T. Li, Y. Luo, N. Li, B. Tang, Y. Liu, S. Gao, A. A. Alshehri, I. Shakir, P. O. Agboola, Q. Kong, Q. Wang, D. Ma and X. Sun, *Small*, 2022, **18,** 2106961.